Nanoscale

PAPER

View Article Online
View Journal | View Issue

Cite this: *Nanoscale*, 2014, **6**, 3742

Tumor targeting profiling of hyaluronan-coated lipid based-nanoparticles†

Shoshy Mizrahy,[abc] Meir Goldsmith,[abc] Shani Leviatan-Ben-Arye,[abc] Einat Kisin-Finfer,[d] Orit Redy,[d] Srimeenakshi Srinivasan,[e] Doron Shabat,[d] Biana Godin[e] and Dan Peer*[abc]

Received 16th November 2013
Accepted 8th January 2014

DOI: 10.1039/c3nr06102g

www.rsc.org/nanoscale

Hyaluronan (HA), a naturally occurring high Mw (HMw) glycosaminoglycan, has been shown to play crucial roles in cell growth, embryonic development, healing processes, inflammation, and tumor development and progression. Low Mw (LMw, <10 kDa) HA has been reported to provoke inflammatory responses, such as induction of cytokines, chemokines, reactive nitrogen species and growth factors. Herein, we prepared and characterized two types of HA coated (LMw and HMw) lipid-based targeted and stabilized nanoparticles (tsNPs) and tested their binding to tumor cells expressing the HA receptor (CD44), systemic immunotoxicity, and biodistribution in tumor bearing mice. *In vitro*, the Mw of the surface anchored HA had a significant influence on the affinity towards CD44 on B16F10 murine melanoma cells. LMw HA–tsNPs exhibited weak binding, while binding of tsNPs coated with HMw HA was characterized by high binding. Both types of tsNPs had no measured effect on cytokine induction *in vivo* following intravenous administration to healthy C57BL/6 mice suggesting no immune activation. HMw HA–tsNPs showed enhanced circulation time and tumor targeting specificity, mainly by accumulating in the tumor and its vicinity compared with LMw HA–tsNPs. Finally, we show that methotrexate (MTX), a drug commonly used in cancer chemotherapy, entrapped in HMw HA–tsNPs slowly diffused from the particles with a half-life of 13.75 days, and improved the therapeutic outcome in a murine B16F10 melanoma model compared with NPs suggesting an active cellular targeting beyond the Enhanced Permeability and Retention (EPR) effect. Taken together, these findings have major implications for the use of high molecular weight HA in nanomedicine as a selective and safe active cellular targeting moiety.

1. Introduction

Hyaluronan (HA) is a naturally occurring linear glycosaminoglycan (GAG) composing parts of the extracellular matrix (ECM). HA is comprised of alternating disaccharide units of D-glucuronic acid and *N*-acetyl-D-glucosamine with a β-(1–4) interglycosidic linkage.[1] HA was first considered to play mainly a structural role due to the outstanding hydrodynamic properties especially related to its viscosity and ability to retain water.[2] However, over the years many additional roles of HA have been revealed such as its crucial involvement in cell growth, embryonic development, healing processes, inflammation, and tumor development.[2,3]

As with other components of the ECM, low Mw (LMw) fragments of HA were reported to act as mediators of inflammation.[4] This is opposed to the non-immunogenic and anti-angiogenic characteristics of high Mw (HMw) HA.[5] The different biological effects reported for HMw and LMw HA have been suggested to be mediated by the HA cell surface receptor CD44. We and others have demonstrated that there is a direct correlation between HA Mw and its affinity towards CD44.[6–8] The high affinity of HMw HA (as opposed to the low affinity of LMw HA) is probably a result of multivalent binding as HMw HA contains thousands of binding sites. Additional factors also regulate HA–CD44 interaction among which are the surface density of CD44, its many splice variants and most likely different conformations.[9]

However, there is inconsistency in the literature regarding the dependency of HA Mw on the biological functions with respect to inflammation and tumor progression as administration of LMw HA to tumor xenografts inhibits rather than stimulating tumor growth, and overexpression of hyaluronidase suppresses colon and breast carcinoma growth in human

[a]*Laboratory of NanoMedicine, Department of Cell Research and Immunology, George S. Wise Faculty of Life Science, Tel Aviv University, Tel Aviv 69978, Israel. E-mail: peer@tauex.tau.ac.il*

[b]*Department of Materials Science and Engineering, Faculty of Engineering, Tel Aviv University, Tel Aviv 69978, Israel*

[c]*Center for Nanoscience and Nanotechnology, Tel Aviv University, Tel Aviv 69978, Israel*

[d]*School of Chemistry, Tel Aviv University, Tel Aviv 69978, Israel*

[e]*Houston Methodist Research Institute, Houston, TX, 77030, USA*

† Electronic supplementary information (ESI) available. See DOI: 10.1039/c3nr06102g

xenografts.[2] In addition, reports regarding induction of inflammatory cytokines as a result of LMw HA administration are also inconsistent.[10] Several factors may contribute to these[5] inconsistent reports, including non-HA contamination (for HA samples of animal or bacterial origin) and the fact that all evidence of the biological effects of LMw HA fragments was based on exogenous addition of HA fragments.

There are several advantages of HMw HA, which make it suitable for use in drug delivery systems (DDS): solubility in water, biodegradability, biocompatibility, lack of toxicity and immunogenicity, and the ease of chemical modification.[3] As a coating agent for DDS, HMw HA promotes long-term circulation and increased stability that can be attributed to reduction in protein adsorption (corona) and opsonisation.[11] This feature was successfully adopted from the HA capsule of group A streptococci that enables it to escape the host immune response.[12] In addition, as the major ligand for CD44 and CD168 (also known as Receptor for Hyaluronan Mediated Motility, RHAMM), HA is suitable for targeting CD44 and RHAMM-expressing cells.[3] Since both CD44 and CD168 are overexpressed on various tumors, for example, squamous cell carcinoma, ovarian, colon, stomach, glioma, and many types of leukemia, lymphoma and multiple myeloma, the use of HA as a targeting agent is even more attractive.[11] We and others have demonstrated that HA can be covalently attached to the surface of nanoparticles (NPs) and efficiently target epithelial cancer cells and leukocytes expressing HA receptors.[3,13–18]

Our previous report focused on the design and characterization of a small library of lipid-based-nanoparticles distinguished by the length of their surface anchored HA, ranging from 6.4 kDa to 1500 kDa.[7] We have shown that the affinity of the targeted and stabilized nanoparticles (tsNPs) towards the CD44 receptor was found to be solely controlled by the Mw of the tsNP surface bound HA, from extremely low binding for LMw HA to binding with high affinity for HMw HA by Surface Plasmon Resonance (SPR) analysis.

In this study, we focused on two tsNPs having various Mw of anchored HA on their surface, LMw HA (<10 kDa) and tsNP HMw HA (>700 kDa). The effects of HA Mw on cell binding, immune response, circulation time and tumor localization as well as therapeutic response with MTX as a model drug entrapped in the NPs are investigated and discussed.

2. Experimental

2.1 Materials

Pure soybean phosphatidylcholine (Phospholipon 90G) was a kind gift from Phospholipid GMBH (Germany). 1,2-Dipalmitoyl-*sn-glycero*-3-phosphoethanolamine (DPPE) and cholesterol (Chol) were purchased from Avanti Polar Lipids Inc. (Alabaster, AL, USA). Sodium hyaluronate with an average Mw of 6.4 kDa and 700 kDa was purchased from Lifecore Biomedical, LLC (MN, USA). Methotrexate (MTX), ethyl-dimethyl-aminopropyl-carbodiimide (EDC), LPS, paraformaldehyde (PFA) and trypan blue were purchased from Sigma-Aldrich Co. (St Louis, MO, USA). Sulfo-NHS was purchased from Proteochem. Concanavalin A-labeled Alexa 488 (ConA 488) was purchased from Life Technologies. 2-(4-Morpholino)ethane sulfonic acid (MES) was purchased from Fisher Scientific. Alexa Fluor 488 rat anti-human CD44 (clone # IM7) and IgG2b isotype control antibodies were purchased from BioLegend (San Diego, USA). The Milliplex® MAP kit 25-plex Mouse cytokine/chemokine Magnetic bead panel (MCYTOMAG-70K-PMX) was purchased from Millipore. Materials for cell cultures, HEPES buffer and EZ-PCR Mycoplasma Test Kit were purchased from Biological Industries Co. (Beit Haemek, Israel). Tissue-Tek OCT was purchased from Sakura. Fluorescent mounting medium was purchased from Golden Bridge International, Mukilteo, WA, USA. All other reagents were of analytical grade.

2.2 Methods

2.2.1 Cy5–DPPE conjugate synthesis. Cy5-NHS was synthesized according to a previously published procedure.[19]

Cy5-NHS (27 mg, 0.043 mmol) was dissolved in 2 ml of DMF and 1 ml of $CHCl_3$. Then 1,2-dipalmitoyl-*sn-glycero*-3-phosphoethanolamine (DPPE) (30 mg, 0.043 mmol) was added followed by the addition of Et_3N (5.9 μL, 0.043 mmol). The reaction mixture was heated to 70 °C and stirred overnight. The reaction was monitored by RP-HPLC (gradient 10–90% ACN in H_2O, 20 min). Upon completion, the solvent was removed under reduced pressure and the crude product was purified by column chromatography on silica gel (3 : 7 MeOH : DCM) to afford the Cy5–DPPE conjugate (45 mg, 89%) as a blue solid (see Scheme 1).

^{1}H NMR (400 MHz, $CDCl_3$): δ = 8.35 (1H, brs), 7.86 (2H, quart, J = 8.8 Hz), 7.39–7.32 (4H, m), 7.24–7.15 (4H, m), 7.09 (1H, d, J = 7.8 Hz), 6.94 (1H, t, J = 9.5 Hz), 6.52 (1H, d, J = 13.3 Hz), 6.40 (1H, d, J = 13.3 Hz), 5.22 (1H, m), 4.41 (1H, dd, J = 11.8, 3 Hz), 4.19–4.10 (5H, m), 4.05–4.02 (4H, m), 3.48 (2H, m), 2.32–2.22 (6H, m), 1.85 (2H, m), 1.77–1.72 (2H, m), 1.70 (6H, s), 1.69 (6H, s), 1.55–1.53 (4H, m), 1.40–1.36 (2H, m), 1.23 (48H, m), 0.87 (9H, m). MS (ES^-): m/z calc. for $C_{70}H_{112}N_3O_9P$: 1169.8; found: 1171.1 $(M + H)^+$. HPLC grad. 10–90% ACN in water 20 min, retention time – 14.5 min, λ = 640 nm.

2.2.2 Preparation of lipid NPs and encapsulation of MTX. Multilamellar vesicles (MLVs) composed of PC : Chol : DPPE at a molar ratio of 60 : 20 : 20 were prepared by the traditional lipid-film method.[16,17,20,21] MLVs prepared for confocal analysis contained 0.1% Cy5 labeled DPPE. Briefly, the lipids were dissolved in ethanol, evaporated to dryness under reduced pressure in a rotary evaporator (Buchi Rotary Evaporator Vacuum System Flawil, Switzerland) and hydrated by the PBS swelling solution at pH 7.4 or with MTX (1.5 mg ml^{-1}) in PBS solution at pH 7.4. This was followed by extensive agitation using a vortex device and 2 h of incubation in a shaker bath at 37 °C. The MLVs

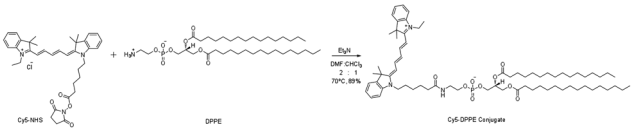

Scheme 1 Chemical synthesis of the Cy5–DPPE conjugate.

were extruded through a Lipex extrusion device (Northern lipids, Vancouver, Canada), operated at 65 °C and under a nitrogen pressure of 200–500 psi. The extrusion was carried out in stages using progressively smaller pore-size polycarbonate membranes (Whatman Inc., UK), with several cycles per pore-size, to achieve unilamellar vesicles in a final size range of ~100 nm in diameter. The lipid mass was quantified as previously reported.[17] MTX was assayed at 303 nm using a UV spectrophotometer (Cary 5000).

2.2.3 Surface modification of NPs. The surface modification was carried out on the NPs, according to our previously reported procedures.[22] Briefly, HMw HA (700 kDa) or LMw HA (8.9 kDa) (Lifecore Biomedical LLC, Chaska, MN, USA) was dissolved in 0.2 M MES buffer (pH 5.5) to a final concentration of 5 mg ml^{-1}. HA was activated with EDC and sulfo-NHS at a molar ratio of 1 : 1 : 6. After 30 min of activation the lipid NPs were added and the pH was adjusted to 7.4. The solution was incubated at room temperature for 2 h. The free HA was removed by 3 cycles of repeated washing by centrifugation ($1.3 \times 10^5 g$, 4 °C, 60 min).

2.2.4 Entrapment of MTX in tsNPs and release profile. The kinetics of drug efflux was studied as previously described.[15–18] Briefly, a suspension of tsNPs or NPs (0.5–1.0 ml) was placed in a dialysis sac and the sac was immersed in a continuously stirred receiver vessel, containing drug-free buffer (HBS at pH 7.4). The buffer volume in the receiver vessel was 10- to 16-fold higher than that of the tsNP sample in the dialysis sac. At designated periods, the dialysis sac was transferred from one receiver vessel to another, containing fresh (*i.e.*, drug-free) buffer. Drug concentration was assayed in each dialysate and in the sac (at the beginning and end of each experiment). In order to obtain a quantitative evaluation of drug release, experimental data were analyzed according to a previously derived multi-pool kinetic model,[21,23] in which drug efflux from the sac into the reservoir occurs from a series of independent drug pools, one corresponding to the free (*i.e.*, unencapsulated) drug, and all others to the tsNP-associated drug. The overall drug release corresponds to the following equation:

$$f(t) = \sum_{j=1}^{n} f_j\left(1 - \exp^{-k_j t}\right) \quad (1)$$

where t denotes the time, $f(t)$ is the cumulative drug released into the dialysate at time t, normalized to the total drug in the system at time 0, f_j is the fraction of the total drug in the system occupying the j^{th} pool at time = 0, and k_j is the rate constant for drug diffusion from the j^{th} pool.

The data analysis of efflux kinetics is also used to calculate the encapsulation efficiency. As discussed above, magnitudes of the parameter f_j are obtained through data analysis. When the efflux experiment is carried out on samples from the complete lipid NP preparation, the sum of f_j(s) for the pool(s) of the encapsulated drug is also the efficiency of encapsulation.

MTX concentration was assayed by using a UV spectrophotometer (Cary 5000) at 303 nm.

2.2.5 Particle size distribution and zeta potential measurements. Particle size distribution and zeta potential measurements were determined by light scattering using a Malvern nano ZS Zetasizer (Malvern Instruments Ltd, Worcestershire, UK). Size measurements were performed in HBS pH 7.4 and zeta potential measurements were performed in 0.01× HBS pH 7.4. Each experimental result was an average of at least six independent measurements.

2.2.6 Cell culture growth and maintenance. Monolayers of B16F10 (murine skin melanoma) cells were grown in 100 × 20 mm dishes as previously reported.[17,24] The cells were cultured in Dulbecco's modified Eagle's medium (DMEM) containing 10% fetal bovine serum, penicillin (100 U per ml), streptomycin (0.1 mg ml^{-1}), nystatin (12.5 U per ml) and L-glutamine (2 mM). Cells were free of Mycoplasma contamination as determined by a Mycoplasma PCR test carried out every 3 months. The viability of cultures used in the experiments was >90%, as determined by the trypan blue method.

2.2.7 Flow cytometry analysis of surface CD44. Flow cytometry of cell surface CD44 antigens was performed as previously described.[17,18] The following mAbs were used: Alexa Fluor 488-conjugated rat anti-human CD44 (clone # IM7) and IgG2b isotype control. Data were acquired on a FACScan with CellQuest software (Becton Dickinson, Franklin Lakes, NJ, USA). Data analysis was performed using FlowJo software (Tree Star, Inc., Oregon, USA).

2.2.8 tsNP binding to cell monolayers – confocal microscopy analysis. Analysis of tsNP binding to B16F10 cells was performed in 24 well plates as previously described.[22] Briefly, 7.0 × 10^4 B16F10 cells were seeded on cover slips in growth media. The cells were exposed to Cy5 labeled NPs or tsNPs (25 μg) in medium without serum for a period of 1 h at 37 °C in a humidified atmosphere with 5% CO_2. Subsequently, the cells were washed twice using cold PBS, fixated with 4% PFA and washed again with cold PBS. ConA 488 (Life Technologies) staining was performed according to the manufacturer's instructions. The cells were mounted using the fluorescent mounting medium (Golden Bridge International, Mukilteo, WA, USA) and the fluorescence was assessed using a confocal microscope (LEICA TC SP5 II STED) with a spatial resolution of 50–70 nm. Serial optical sections of the cells were recorded for each treatment and the images were processed using the Leica Application Suite LAS-AF Lite software (Leica Microsystems Inc.).

2.2.9 Animal treatment. Animals were obtained from the Animal Breeding Center, Tel Aviv University (Tel Aviv, Israel). Animals were maintained and treated according to the National Institutes of Health guidelines. All animal protocols were approved by the Tel Aviv Institutional Animal Care and Use Committee.

2.2.10 Cytokine induction assay *in vivo*. NPs or tsNPs were injected intravenously into C57BL mice at a dose of 90 mg kg^{-1}. Lipopolysaccharide (LPS, Sigma) at a concentration of 1 mg ml^{-1} (100 μl) was used as a positive control. Two hours post injection whole blood was collected and the animals were sacrificed. After collection, whole blood was allowed to clot by leaving it undisturbed at RT for 30 minutes. The clot was removed by centrifugation for 10 minutes at 1000 × *g*. The supernatant was transferred to a new tube and stored at −80 °C prior to cytokine analysis.

An hour before the analysis, the samples were thawed, diluted 1 : 2 in the diluent solution provided by the manufacturer and analyzed according to the manufacturer's instructions, using a Milliplex® MAP kit 25-plex Mouse cytokine/chemokine Magnetic bead panel (MCYTOMAG-70K-PMX, Millipore). The following cytokines were assessed: G-CSF, GM-CSF, IFN-γ, IL-10, IL-12 (p40), IL-12 (p70), IL-13, IL-15, IL-17, IL-1α, IL-1β, IL-2, IL-4, IL-5, IL-6, IL-7, IL-9, IP-10, KC, MCP-1, MIP-1α, MIP-1β, MIP-2, RANTES, and TNF-α. Cytokine levels were read on the Luminex 200 System, Multiplex Bio-Assay Analyzer (Millipore, MA, USA). The quantification was done based on standard curves for each cytokine in the concentration range of 3.2–10 000 pg ml^{-1}.

2.2.11 Syngeneic SC tumor model. 10–12 week old female C57BL/6 mice were maintained under specific pathogen-free (SPF) conditions. Tumors were induced by subcutaneous injection of 2×10^5 B16F10 cells in HBSS SC into the flank region of the mice. Tumors reached ~40 to 50 mm^3 10–12 days post injection. For biodistribution studies, Cy5 labeled NPs or tsNPs were injected intravenously (i.v.) into tumor bearing mice using a 27-gauge needle at a dose of 90 mg kg^{-1}. 3.5, 24 and 48 hours post injection the mice were sacrificed and the liver, lungs, spleen, heart and kidneys were isolated and scaled organ fluorescent signals per area were analyzed using the Maestro *in vivo* fluorescence imaging system (Perkin Elmer, Inc.).

For histological hematoxylin and eosin (H&E) analysis tumors were fixed in 10% formalin in PBS overnight at RT, embedded in paraffin and cut into 5 μm sections.

For determination of NP and tsNP tumor localization, tumors were isolated 3.5, 24 and 48 hours post NP or tsNP injection. The tumors were fixed in 10% buffered formalin in PBS ON at RT and transferred to 30% buffered formalin overnight at 4 °C. The tumors were embedded in OCT and cut into 5 μm sections. Images were obtained using the confocal microscope LEICA TC SP5 II STED with a spatial resolution of 50–70 nm. Tumor fluorescence signals per area were analyzed using the Leica Application Suite LAS-AF Lite software.

2.2.12 Therapeutic efficacy studies. Treatments were initiated 12 days post tumor inoculation, when tumor volumes reached ~40 mm^3 (day 0). The tumor volume was calculated as: $(\text{width})^2 \times \text{length}/2$. The mice were randomly separated into four groups ($n = 6$ per group): (1) HBS, (2) free MTX, (3) NPs entrapping MTX, (4) LMw HA–tsNPs entrapping MTX and (5) HMw HA–tsNPs entrapping MTX. The doses in the free MTX and in all the tsNP formulations were 0.25 mg kg^{-1} body and treatments were given every other day for 5 times. Administration was by i.v. injection of 100 μl of the selected formulation to the lateral tail vein, using a 27-gauge needle. Tumor dimensions were assayed by using an electronic caliper as previously reported.[16,18]

2.2.13 Statistical analysis. Results are expressed as mean ± SD. Differences between two means were tested using an unpaired, two-sided Student's *t*-test. Differences between treatment groups were evaluated by one-way ANOVA with significance determined by the Bonferroni adjusted *t*-test.

3. Results and discussion

3.1 Structural characterization of NPs and tsNPs

In order to investigate the effect of surface anchored HA Mw on NP cellular targeting, biodistribution and immune modulation, we prepared three types of NPs: uncoated lipid NPs, lipid NPs coated with LMw HA (LMw HA–tsNPs) and lipid NPs coated with HMw HA (HMw HA–tsNPs). The structural characteristics of all NPs are summarized in Table 1.

Surface modification of lipid NPs with HA did not lead to a significant change in NP size, however, a significant decrease in the zeta potential of the NPs was detected from −8 mV to <−21 mV. This decrease in the zeta potential is in line with the surface modification with the negatively charged HA.

3.2 HMw HA–tsNPs selectively bind to B16F10 cells *in vitro*

The covalent attachment of HA to the surface of the NPs did not impair the ability to bind to the CD44 receptor, as we have shown previously.[7] As we have reported, coating NPs with HA provokes their binding to recombinant human CD44-Fc chimera immobilized to a carboxymethylated dextran sensor chip (CM5) using SPR analysis.[7] We have demonstrated that the affinity of tsNPs towards the immobilized CD44 was solely controlled by the Mw of the surface anchored HA. While LMw HA–tsNPs were characterized by extremely low binding, HMw HA–tsNPs bind to the immobilized CD44 with high affinity.

Here we present the effect of anchored HA Mw on binding to B16F10 cells (Fig. 1). B16F10 cells were used due to the high expression of the HA receptor CD44, a feature of many cancer cells. The expression level of CD44 in B16F10 was demonstrated by flow cytometry as described in the Experimental section (Fig. 1A).

In order to test the NPs and tsNPs in an *in vitro* setting, one of the lipids (DPPE) in the formulation (both in NPs and tsNPs) was labeled with Cy5 and incorporated into the preparation of the NPs (at 0.1% mol). The cells were incubated in the presence of tsNPs for 1 h at 37 °C as described in the Experimental section and the binding of tsNPs was analyzed by confocal microscopy. As seen in Fig. 1B, surface bound HA retained its affinity towards the HA receptor CD44 and this affinity is directly related to the Mw of the surface HA. While the Cy5 labeling is hardly detectable for cells incubated with NPs or LMw HA–tsNPs, incubation with HMw HA–tsNPs resulted in

Table 1 Physicochemical characteristics of NPs, tsNPs coated with LMw HA and tsNPs coated with HMw HA. The measurements were performed using a Malvern Nano ZS zetasizer as described in the Materials and methods section[a]

Particle	Hydrodynamic diameter (nm)	Zeta potential (mV)
NPs	166 ± 20	−8.4 ± 2.5
LMw HA–tsNPs	169 ± 25	−21.2 ± 3.5
HMw HA–tsNPs	190 ± 35	−22.7 ± 3

[a] Each result is an average ± SD of at least 6 independent measurements. Batch-to-batch variability was small, within the range reported for this particular batch.

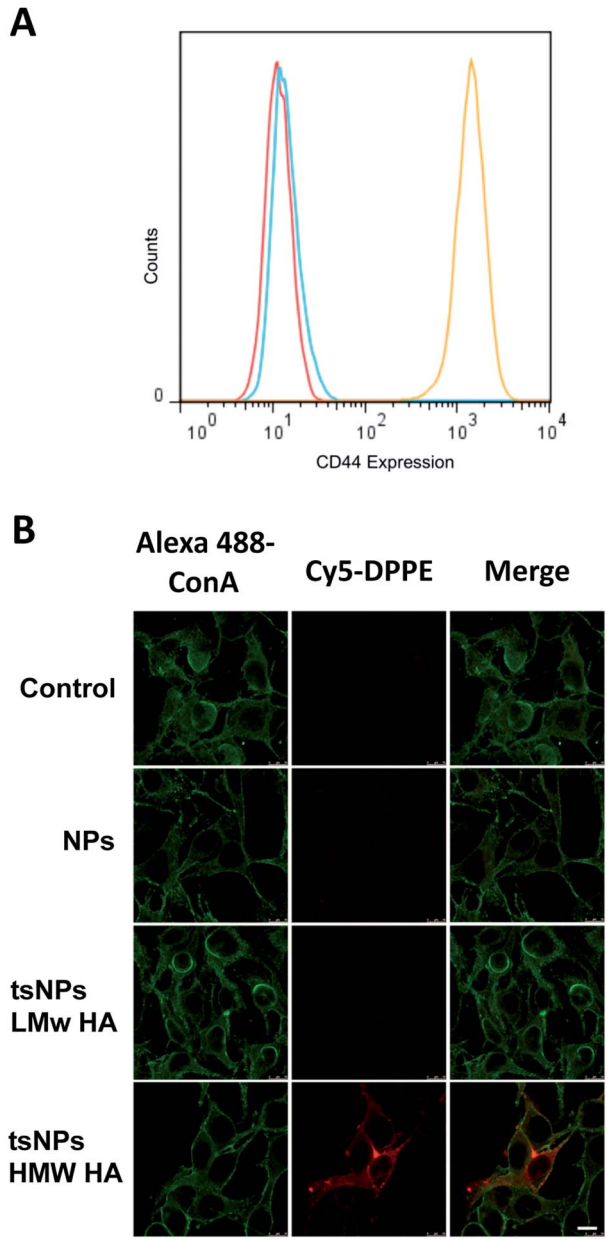

Fig. 1 HMw HA–tsNPs selectively bind to B16F10 cells. (A) A representative FACS histogram of CD44 expression in B16F10 cells is presented. Cells were stained with the isotype control antibody (blue curve), or with Alexa Fluor 488 anti CD44 and IgG2b isotype control. Control, non-stained cells are presented by the red curve. (B) Representative confocal images of binding of Cy5 labeled NPs and tsNPs to B16F10 cells. Cells were seeded onto 6 well pates and incubated with 25 μg of Cy5 labeled NP LMw HA–tsNPs or HMw HA–tsNPs for 1 h at 37 °C. Cell membranes were labeled with Alexa 488 ConA. Bar 10 μm.

significant fluorescence mostly at the cell membrane. This clearly indicates specific binding of the HMw HA–tsNPs and correlates with our previously obtained SPR results.[7]

3.3 tsNPs do not trigger cytokine release when injected systemically

Unlike LMw HA that has shown to induce inflammatory responses, HMw HA is believed to play a homeostatic role.[25] As was shown for fragments of other extracellular matrix (ECM) components,[4] upon tissue destruction, HMw HA is broken down to fragments that can activate inflammatory responses. LMw HA was shown to stimulate macrophages recruited to the sites of inflammation and to produce important mediators of tissue injury and repair.[26–28] In addition to macrophages, several studies demonstrated induction of pro-inflammatory responses by LMw HA of other cell types such as epithelial cells, endothelial cells, fibroblasts, and dendritic cells.[25] The genes induced by LMw HA include the cytokines (TNF-α, IL-6, IL-12 and IL-8), chemokines (MIP-1α, MIP-1β, KC, RANTES, MCP-1, and IFN-inducible protein-10), reactive nitrogen species and several growth factors.[25,26,29]

Nevertheless, literature reports regarding general pro-inflammatory effects by HA and specific effects on macrophage activation are not consistent. HMw HA has shown to induce TNF-α production by the RAW 264.7 cell line and by primary (peritoneal) macrophages[30] while in another study that was also performed on the RAW 264.7 cell line there was no induction of pro-inflammatory cytokines regardless of the HA Mw tested.[10]

Therefore, we have previously tested whether tsNPs with different surface anchored HA Mws can induce macrophage activation.[7] We monitored the levels of secreted TNF-α and IL-10 from RAW 264.7 macrophages following incubation with NPs or tsNPs. We chose to monitor the levels of TNF-α since it is the first cytokine to be released after activation of essentially all Toll-Like Receptors (TLRs) and is regarded as the key pro-inflammatory cytokine.[20,31] In addition, TNF-α also enhances the production of the key anti-inflammatory cytokine IL-10,[32] which in turn suppresses TNF-α to complete the negative regulatory feedback cycle. No cytokine induction was observed regardless of the HA Mw anchored to the NPs' surface.[7]

In this study, we tested the effect of NPs and tsNPs on induction of cytokines *in vivo* upon a single intravenous (i.v.) administration. For this task, NPs and tsNPs were injected i.v. into C57BL mice. LPS, a potent TLR4 activator that mediates acute inflammation,[27,33,34] was used as the positive control.[33] Serum cytokine levels were measured using a Milliplex® MAP kit 25-plex Mouse cytokine/chemokine Magnetic bead panel as described in the Experimental section (Fig. 2). In order to achieve a better understanding of the influence of the NPs and tsNPs on the immune response, the cytokine panel measured was largely extended in comparison to our previous study and included the following cytokines, chemokines and growth factors: TNF-α, INF-γ, IL-2, IL-1β, IL-12 (p40), IL-12 (p70), IL-6, IL-4, IL-7, IL-5, IL-9, IL-10, IL-15, IL-13, IL-17, KC, MIP2-a, IP-10, MCP-1, MIP-1α, MIP-1β, RANTES, G-CSF and GM-CSF (Fig. 2). No induction of cytokines was observed regardless of the surface HA Mw of the tsNPs. These results contradict previous studies, which related LMw HA with macrophage activation and induction of cytokines. However, the result can be explained by the fact that the HA tested was covalently attached to the surface of the lipid NPs by a stable amide bond. Bound HA may be less potent in comparison to free HA as it can hurdle processing by cells and as a result impair macrophage activation. The discrepancy regarding the influence of LMw HA on the immune response should also be addressed. Stern *et al.*[5] discussed this

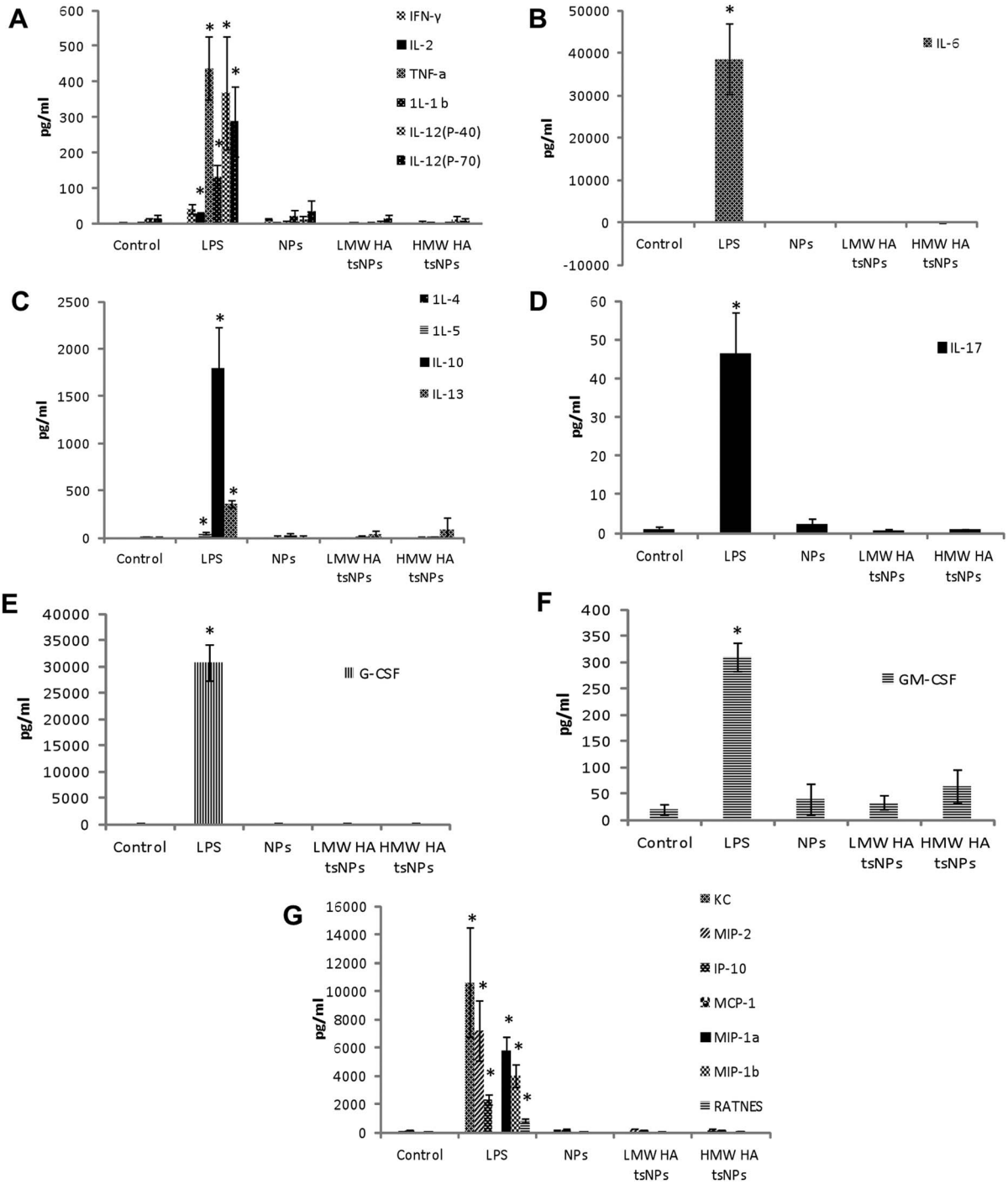

Fig. 2 tsNPs do not trigger cytokine release when injected systemically. NPs and tsNPs were injected i.v. into C57BL mice. Two hours post injection, serum was isolated and cytokine levels were measured using ELISA. (A and B) Pro-inflammatory cytokines and Th1 response. (C) Th2 response, (D) Th17 response. (E–G) Growth factors and chemokines. * denoted $p < 0.05$.

issue and detailed several intrinsic challenges to the study of HA fragments. These challenges include inaccurate measurements of HA fragment Mw, HA sample preparation as it may affect HA conformation and non-HA contamination for HA of animal or bacterial origin.[5] In addition, all evidence of the biological effects of HA fragments was based on exogenous addition of HA fragments and no evidence exists regarding the ability of cells to release, synthesize or even internalize LMw HA.[5]

3.4 HMw HA–tsNPs accumulate in B16F10 tumor bearing mice

3.4.1 Establishment of a syngeneic subcutaneous tumor model. In order to test differences in biodistribution of NPs and tsNPs in solid tumors we have established a syngeneic subcutaneous (SC) B16F10 tumor model in C57BL mice. The syngeneic tumor model offers several advantages over human

xenograft models. It is reproducible, enables use of immunocompetent hosts and therefore better represents natural tumor surroundings and it is generally non-immunogenic.[35] The main disadvantages of syngeneic tumor models are that the tumor cells are rodent, and therefore express the mouse/rat homologues of the desired targets.[35] However, in our case this disadvantage is not relevant as the ligand for both murine and human CD44 is hyaluronan. For this purpose, the highly expressing CD44 cells B16F10 (Fig. 1A) were injected SC and tumors were formed 10–12 days post injection. The obtained tumors contained multiple newly formed blood vessels (Fig. 3), thus this is an ideal model to test the EPR effect of small NPs and the contribution of HA as the coating ligand to target the tumor *via* passive (EPR) and active cellular targeting mechanisms. Pathology examination revealed SC tumors in the mice injected with B16F10 cells whereas their lungs, spleens, kidneys, and livers were found to be tumor-free.

3.4.2 tsNPs are detected in organs after 48 h post administration in B16F10 tumor bearing mice. Literature reports that discuss the influence of free HA Mw on biodistribution performed in healthy mice/rats[36,37] revealed longer circulation time for the HMw HA. In addition, there were differences in the biodistribution. Higher amounts of HMw HA–^{111}In-DTPA conjugates were taken up by the liver in comparison to the LMw HA–^{111}In-DTPA conjugates that were found in the urine probably due to non-enzymatic cleavage.[37] Upon conjugation to the surface of NPs, HMw HA have been shown to significantly increase the NPs' circulation time as it provides a protective hydrophilic coating, similar to the frequently used polyethylene glycol (PEG) and inhibits reticuloendothelial system (RES) uptake.[15,16] In order to test the differences in the biodistribution profile between NPs and tsNPs in tumor bearing mice, Cy5 labeled NPs and tsNPs were injected i.v. and the fluorescence intensity of isolated organs was measured 3.5 and 24 hours post injection by the Maestro *in vivo* fluorescence imaging system (Fig. 4). The NPs and tsNPs were labeled by incorporation of Cy5 conjugated-DPPE that was incorporated into the lipid mixture of the NPs as detailed in the Experimental section. No significant difference in the signals of isolated RES organs (liver, spleen, and lungs) from tumor bearing mice was observed between NPs, HMw HA–tsNPs and LMw-HA–tsNPs at the measured time points (ESI Fig. 1 and 4†).

3.5 HMw HA–tsNPs specifically target B16F10 tumor bearing mice

In order to test the effect of NPs and tsNPs on tumor localization, Cy5 labeled NPs and tsNPs were injected i.v. into B16F10 tumor bearing mice. Tumors were isolated and the signals were analyzed by confocal microscopy as detailed in the Methods section (Fig. 5). The highest tumor signals were obtained with HMw HA coated tsNPs at all time points tested (3.5 h, 24 h and 48 h) (Fig. 5). This can be attributed to a combination of passive targeting *via* the enhanced permeability and retention (EPR) effect that characterizes the solid tumor and active targeting towards the HA receptor CD44 highly expressed on B16F10 cells (Fig. 1). The effect of NP surface anchored HMw HA on promoting long circulation of NPs has been shown[15] and is related to the hydroxyl residues of HA that endow the NPs with a hydrophilic coat that reduces the attachment of circulating serum opsonins and subsequent clearance by the reticuloendothelial system (RES).

The difference between LMw-HA–tsNPs and HMw-HA–tsNPs can be explained by the significantly lower binding to CD44 as shown also in Fig. 1 and our previously reported Surface Plasmon Resonance (SPR) data.[7] This can highlight the importance of active tumor targeting *via* the CD44 receptor for promoting long circulation beyond the passive targeting obtained by the EPR effect alone.

The LMw HA coating on the NPs increases the tumor localization signal, however the difference between NPs and LMw HA coated NPs is not significant.

3.6 HMw HA–tsNPs entrapping MTX enhance the therapeutic response in B16F10 melanoma bearing mice

After confirming that there is no statistical difference between tumor accumulation of NPs and LMw HA–tsNPs 48 h post i.v. administration and substantial accumulation of the HMw HA–tsNPs in the tumor, we hypothesize that entrapping a therapeutic payload within the HMw HA–tsNPs should show an improved therapeutic response which is beyond the effect of the EPR. The hydrophilic chemotherapy drug MTX was chosen as a surrogate marker to test this hypothesis. We tested *in vivo* the following groups: mock-treated, free MTX,

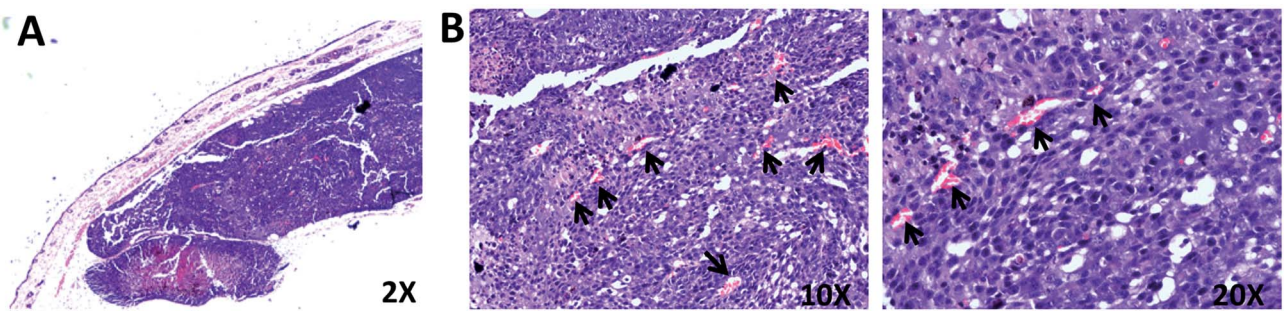

Fig. 3 H&E staining of SC B16F10 tumors. (A) Representative image of the B16F10 SC tumor. (B) Tumor vasculature. The arrows indicate newly formed blood vessels. 2×10^5 B16F10 cells were injected subcutaneously into C57BL mice. The tumors were removed 7 days post cell injection, fixed in formaldehyde and embedded in parathion. Sections were stained with H&E.

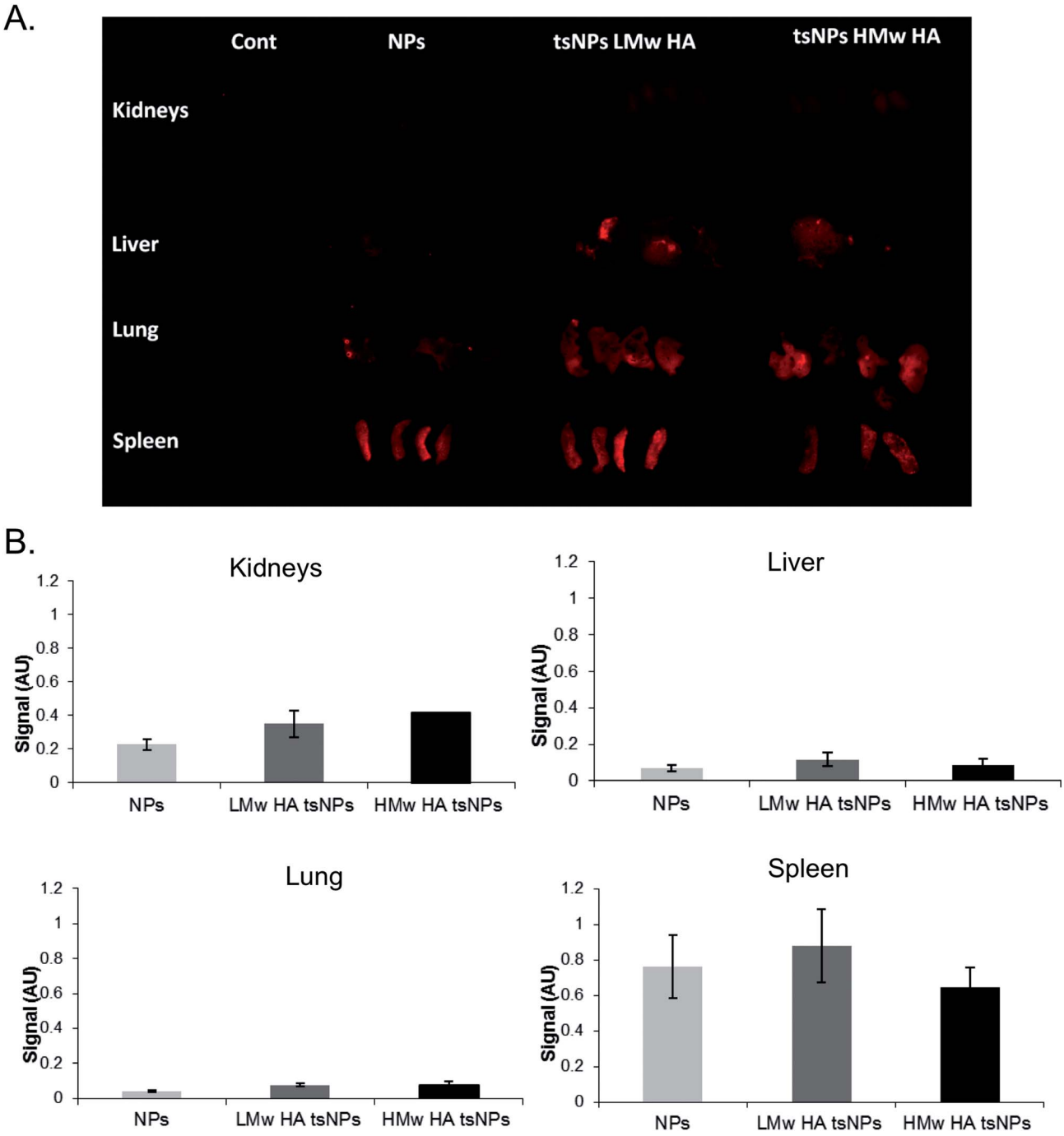

Fig. 4 Biodistribution of NPs and tsNPs in B16F10 SC tumor bearing mice. Mice were injected with PBS, Cy5 labeled NPs or tsNPs. 24 hours post injection mice organs were isolated and fluorescent signals were measured as described in the Experimental section. (A) Isolated organs. (B) The scaled fluorescent signal levels per area of isolated organs were measured by the Maestro *in vivo* fluorescence imaging system.

NPs entrapping MTX, LMw HA–tsNPs entrapping MTX and HMw HA–tsNPs entrapping MTX.

We first entrapped MTX in the particles and characterized their size distribution and zeta potential (Table 2).

Encapsulation of MTX did not change significantly the size distribution of the particles (Table 2) nor their zeta potential indicating that the drug is entrapped in the aqueous phase of the particles. The measured zeta potential of LMw HA–tsNPs and HMw HA–tsNPs was similar (Table 2). This is an expected observation since the amount of carboxyl group is similar for HMw HA and LMw HA since we used equal weights and was already observed for the particles without the entrapped drug (Table 1).

Next, we monitored the drug release profile *in vitro* as detailed in the Experimental section.

The MTX release profile from the NPs, LMw HA–tsNPs and HMw HA–tsNPs (Fig. 6A) was processed according to eqn (1) and found to fit the case of 2 drug pools (*i.e.*, $n = 2$) with a rather fast

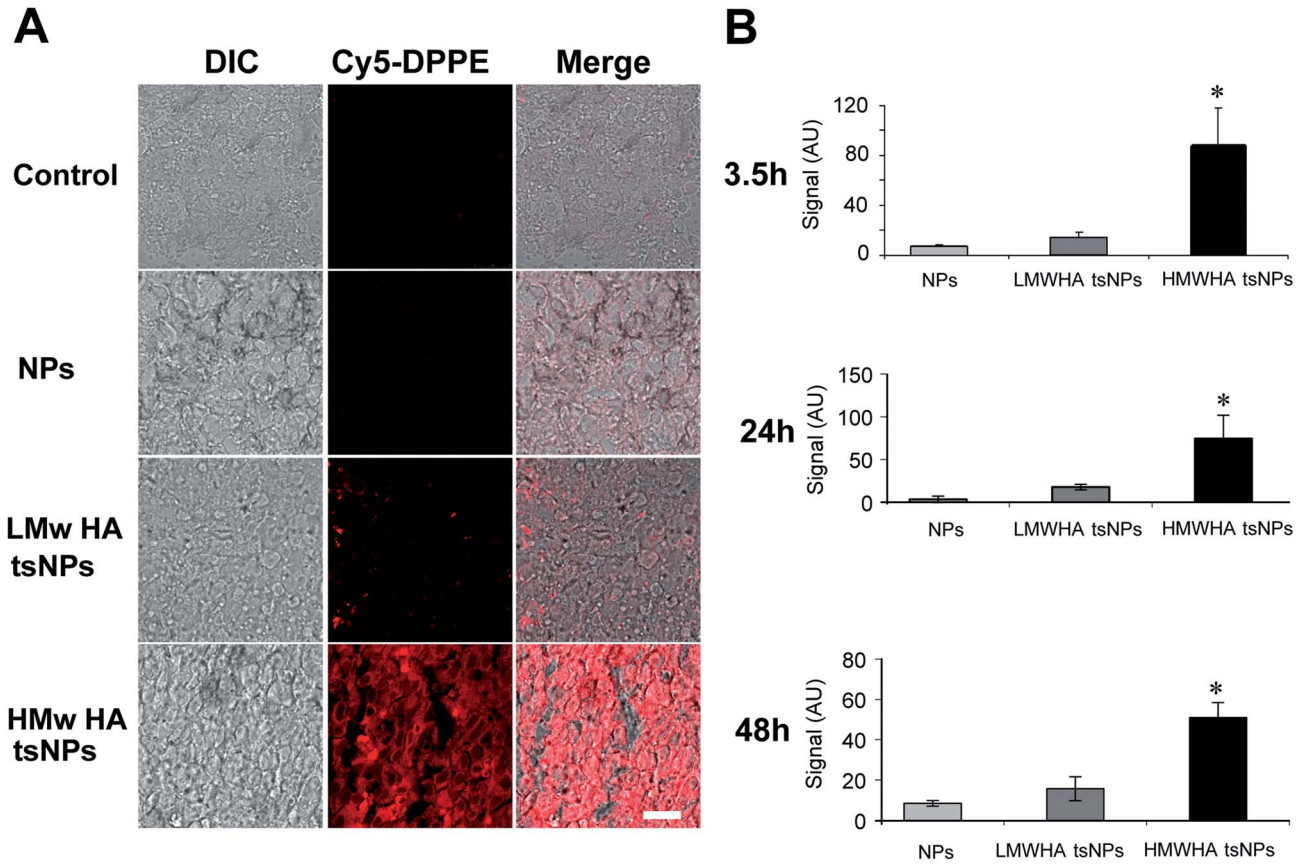

Fig. 5 Tumor localization of NPs and tsNPs post intravenous injection. (A) Representative confocal images of B16F10 isolated tumors 24 h post i.v. injection of Cy5 labeled NP and tsNPs. Bar scale 25 μm. B16F10 tumor bearing mice were i.v. injected with Cy5 labeled NPs and tsNPs. 24 hours post injection tumors were isolated, fixed in formalin and embedded in OCT. Sections were analyzed by confocal microscopy as described in the Experimental section. (B) Representative tumor fluorescent signals per area obtained from confocal analysis 3.5, 24 and 48 hours post i.v. injection of Cy5 labeled NPs and tsNPs to B16F10 tumor bearing mice.

dissipation of unencapsulated MTX and significantly slower efflux of the encapsulated MTX. The rate constant determined for the efflux of encapsulated MTX from NPs, LMw HA–tsNPs and HMw HA–tsNPs was 2.8×10^{-3} per hour, 2.6×10^{-3} per hour and 2.2×10^{-3} per hour corresponding to half-lives of 10, 11 and 13.75 days, respectively. It is likely that the high molecular weight HA serves as an additional reservoir of MTX since the diffusion of MTX from these particles is substantially slower than from LMw HA–tsNPs or the non-coated NPs. The MTX encapsulation efficiency was 60(±4)%, 63(±2)% and 69.4(±5.5)% for NPs, LMw HA–tsNPs and HMw HA–tsNPs, respectively.

Table 2 Physicochemical characteristics of NPs and tsNPs coated with LMw HA or HMw HA entrapping MTX. The measurements were performed using a Malvern Nano ZS zetasizer as described in the Materials and methods section[a]

Particle	Hydrodynamic diameter (nm)	Zeta potential (mV)
NPs (MTX)	159 ± 28	−7.8 ± 1.5
LMw HA–tsNPs	167 ± 11	−22.1 ± 3.1
HMw-HA–tsNPs (MTX)	189 ± 39	−24.1 ± 4.4

[a] Each result is an average ± SD of at least 6 independent measurements. Batch-to-batch variability was small, within the range reported for this particular batch.

Next, we studied the therapeutic effect of HMw HA–tsNPs entrapping MTX in comparison to the free MTX and of MTX entrapped in NPs in B16F10 bearing mice. Tumors were obtained ~12 days post tumor inoculation, and mice ($n = 6$ per group) were i.v. administrated with: (1) HBS, (2) free MTX, (3) NPs entrapping MTX, (4) LMw HA–tsNPs entrapping MTX and (5) HMw HA–tsNPs entrapping MTX. The doses in the free MTX, NPs and the HMw HA–tsNPs formulations were 0.25 mg kg^{-1} body, and treatments were given every other day for 10 consecutive days starting 7 days post mice randomization. Tumor volumes were monitored every 3 days using an electronic caliper. The MTX entrapped in HMw HA–tsNPs significantly ($p < 0.001$) attenuated the growth of the tumors relative to the free MTX and MTX entrapped in NPs (Fig. 6B) suggesting that EPR is not the dominant mechanism while treating with HMw HA–tsNPs but a combination of EPR (passive tumor targeting) *via* the newly formed blood vessels surrounding the tumor (see Fig. 3) with the active cellular targeting mechanism.

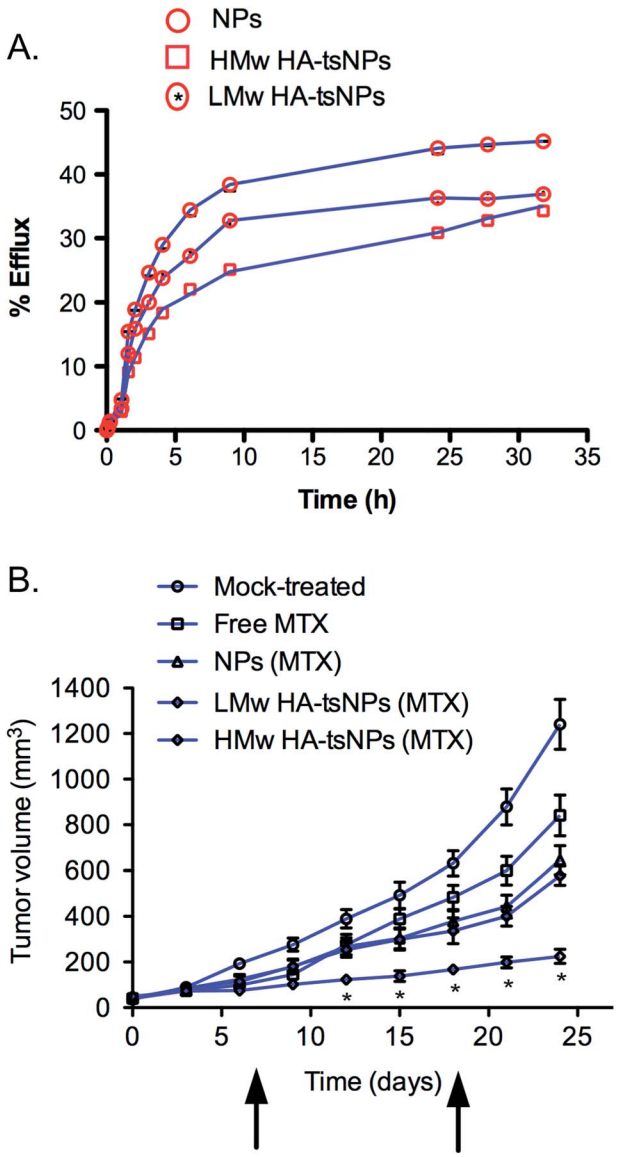

Fig. 6 Enhanced therapeutic response with HMw HA–tsNPs entrapping MTX in a B16F10 melanoma model. (A) MTX release profile from HMw HA–tsNPs and NPs. The points are experimental, each an average of duplicates and the solid curves are the theoretical expectations, the results are of data analysis according to eqn (1) (as described in the Experimental section) for the case of $n = 2$. (B) Therapeutic efficacy was demonstrated using i.v. injections every other day for 5 times post initiation of the experiment with doses and formulations as listed in the Experimental section. Data are expressed as the mean ± SEM of ($n = 6$ per group). * = $p < 0.001$. The arrows represent start and end of treatment.

4. Conclusions

We have presented two types of lipid NPs distinguished only by the Mw of their surface anchored HA: LMw HA–tsNPs (<10 kDa) and HMw HA–tsNPs (700 kDa). The Mw of the surface anchored HA had a significant influence on the affinity towards the HA receptor CD44 on B16F10 murine melanoma cells *in vitro*. LMw HA–tsNPs exhibited weak binding comparable to uncoated NPs while binding of HMw HA–tsNPs was characterized by high affinity. Both types of tsNPs, regardless of their surface anchored HA Mw, had no effect on triggering an immune response as evident by low to minimal cytokine induction *in vivo* following intravenous administration to C57BL mice.

A significant effect of the tsNP surface anchored HA Mw was also detected for tumor targeting and circulation time as the presence and duration of HMw HA–tsNPs greatly exceeded those of LMw HA–tsNPs and uncoated NPs. Finally, we demonstrated *via* an entrapment of MTX, a commonly used chemotherapy drug that the therapeutic effect in tumor bearing mice treated with HMw HA–tsNPs (entrapping MTX) is substantially higher than in any tested control. This highlights the importance of active tumor targeting *via* the HA receptor for promoting long circulation beyond the passive targeting obtained by the EPR effect alone.

Taking together, these data suggest that HMw HA may have important implications for the development of future drug delivery systems using an active cellular targeting approach.

Acknowledgements

S.M. thanks the TAU Nano Center for the Ph.D. fellowship. This work was supported in part by the grants from the Lewis Family Trust, the Israeli Centre of Research Excellence (I-CORE), Gene Regulation in Complex Human Disease, Center no. 41/11; Israel Science Foundation (Award 181/10); FTA: Nanomedicine for Personalized Theranostics, and by The Leona M. and Harry B. Helmsley Nanotechnology Research Fund awarded to D.P.

Notes and references

1 A. Varki, *Essentials of glycobiology*, Cold Spring Harbor Laboratory Press, Cold Spring Harbor, N.Y., 2009.
2 B. P. Toole, *Nat. Rev. Cancer*, 2004, **4**, 528–539.
3 V. M. Platt and F. C. Szoka, Jr, *Mol. Pharmaceutics*, 2008, **5**, 474–486.
4 T. L. Adair-Kirk and R. M. Senior, *Int. J. Biochem. Cell Biol.*, 2008, **40**, 1101–1110.
5 R. Stern, A. A. Asari and K. N. Sugahara, *Eur. J. Cell Biol.*, 2006, **85**, 699–715.
6 P. M. Wolny, S. Banerji, C. Gounou, A. R. Brisson, A. J. Day, D. G. Jackson and R. P. Richter, *J. Biol. Chem.*, 2010, **285**, 30170–30180.
7 S. Mizrahy, S. R. Raz, M. Hasgaard, H. Liu, N. Soffer-Tsur, K. Cohen, R. Dvash, D. Landsman-Milo, M. G. Bremer, S. M. Moghimi and D. Peer, *J. Controlled Release*, 2011, **156**, 231–238.
8 H. Shigeishi, S. Fujimoto, M. Hiraoka, S. Ono, M. Taki, K. Ohta, K. Higashikawa and N. Kamata, *Int. J. Oncol.*, 2009, **34**, 1565–1571.
9 S. Ogino, N. Nishida, R. Umemoto, M. Suzuki, M. Takeda, H. Terasawa, J. Kitayama, M. Matsumoto, H. Hayasaka, M. Miyasaka and I. Shimada, *Structure*, 2010, **18**, 649–656.
10 D. Krejcova, M. Pekarova, B. Safrankova and L. Kubala, *Neuroendocrinol. Lett.*, 2009, **30**(Suppl 1), 106–111.
11 S. Mizrahy and D. Peer, *Chem. Soc. Rev.*, 2012, **41**, 2623–2640.

12 G. Ouskova, B. Spellerberg and P. Prehm, *Glycobiology*, 2004, **14**, 931–938.
13 R. E. Eliaz and F. C. Szoka, Jr, *Cancer Res.*, 2001, **61**, 2592–2601.
14 R. E. Eliaz, S. Nir and F. C. Szoka, Jr, *Methods Enzymol.*, 2004, **387**, 16–33.
15 D. Peer and R. Margalit, *Neoplasia*, 2004, **6**, 343–353.
16 D. Peer and R. Margalit, *Int. J. Cancer*, 2004, **108**, 780–789.
17 D. Peer, E. J. Park, Y. Morishita, C. V. Carman and M. Shimaoka, *Science*, 2008, **319**, 627–630.
18 I. Rivkin, K. Cohen, J. Koffler, D. Melikhov, D. Peer and R. Margalit, *Biomaterials*, 2010, **31**, 7106–7114.
19 M. E. Jung and W. J. Kim, *Bioorg. Med. Chem.*, 2006, **14**, 92–97.
20 R. Kedmi, N. Ben-Arie and D. Peer, *Biomaterials*, 2010, **31**, 6867–6875.
21 D. Peer and R. Margalit, *Arch. Biochem. Biophys.*, 2000, **383**, 185–190.
22 D. Landesman-Milo, M. Goldsmith, S. Leviatan Ben-Arye, B. Witenberg, E. Brown, S. Leibovitch, S. Azriel, S. Tabak, V. Morad and D. Peer, *Cancer Lett.*, 2013, **334**, 221–227.
23 R. Margalit, M. Okon, N. Yerushalmi and E. Avidor, *J. Controlled Release*, 1992, **19**, 275–288.
24 D. Peer, Y. Dekel, D. Melikhov and R. Margalit, *Cancer Res.*, 2004, **64**, 7562–7569.
25 K. A. Scheibner, M. A. Lutz, S. Boodoo, M. J. Fenton, J. D. Powell and M. R. Horton, *J. Immunol.*, 2006, **177**, 1272–1281.
26 M. R. Horton, M. D. Burdick, R. M. Strieter, C. Bao and P. W. Noble, *J. Immunol.*, 1998, **160**, 3023–3030.
27 C. M. McKee, M. B. Penno, M. Cowman, M. D. Burdick, R. M. Strieter, C. Bao and P. W. Noble, *J. Clin. Invest.*, 1996, **98**, 2403–2413.
28 M. R. Horton, C. M. McKee, C. Bao, F. Liao, J. M. Farber, J. Hodge-DuFour, E. Pure, B. L. Oliver, T. M. Wright and P. W. Noble, *J. Biol. Chem.*, 1998, **273**, 35088–35094.
29 H. Yamawaki, S. Hirohata, T. Miyoshi, K. Takahashi, H. Ogawa, R. Shinohata, K. Demircan, S. Kusachi, K. Yamamoto and Y. Ninomiya, *Glycobiology*, 2009, **19**, 83–92.
30 M. J. Wang, J. S. Kuo, W. W. Lee, H. Y. Huang, W. F. Chen and S. Z. Lin, *J. Neurochem.*, 2006, **97**, 857–871.
31 B. Beutler, *Nature*, 2004, **430**, 257–263.
32 D. F. Fiorentino, A. Zlotnik, T. R. Mosmann, M. Howard and A. O'Garra, *J. Immunol.*, 1991, **147**, 3815–3822.
33 D. Jiang, J. Liang, J. Fan, S. Yu, S. Chen, Y. Luo, G. D. Prestwich, M. M. Mascarenhas, H. G. Garg, D. A. Quinn, R. J. Homer, D. R. Goldstein, R. Bucala, P. J. Lee, R. Medzhitov and P. W. Noble, *Nat. Med.*, 2005, **11**, 1173–1179.
34 C. R. Amura, T. Kamei, N. Ito, M. J. Soares and D. C. Morrison, *J. Immunol.*, 1998, **161**, 2552–2560.
35 B. A. Teicher, *Mol. Cancer Ther.*, 2006, **5**, 2435–2443.
36 M. N. Courel, C. Maingonnat, P. Bertrand, C. Chauzy, F. Smadja-Joffe and B. Delpech, *In Vivo*, 2004, **18**, 181–187.
37 E. Svanovsky, V. Velebny, A. Laznickova and M. Laznicek, *Eur. J. Drug Metab. Pharmacokinet.*, 2008, **33**, 149–157.